Composite Structures 230 (2019) 111502

Contents lists available at ScienceDirect

Composite Structures

journal homepage: www.elsevier.com/locate/compstruct

Bistable laminates with non-cylindrical curved shapes

V.S.C. Chillara*, M.J. Dapino

NSF IUCRC on Smart Vehicle Concepts, Department of Mechanical and Aerospace Engineering, The Ohio State University, Columbus, OH 43210, USA

ARTICLE INFO

Keywords:
Bistable
Morphing
Analytical model
Non cylindrical
Non orthogonal
Actuation

ABSTRACT

Thermally-cured fiber-reinforced polymeric laminates can exhibit bistable cylindrical shapes when their plies are configured orthogonally. Such "cross-ply" laminates have been studied extensively through modeling and experiments. However, bistable laminates with non-cylindrical shapes, especially through non-orthogonal ply orientations, have received little attention due to inherent design limitations. This paper presents an approach for developing non-cylindrical curved shapes based on bistability in mechanically-prestressed laminates; prestress is applied by laminating prestrained fiber-reinforced elastomeric laminae on either face of an initially stress-free isotropic layer. An analytical laminated-plate model is developed based on strain energy minimization and stable shapes are calculated for various orientations of the prestrained laminae. The modeled shapes are in agreement with the measured shapes of physical rectangular laminates within 11%. The minimum polynomial order for the calculation of non-cylindrical shapes is fourth; a simplified constitutive model for prestrained-elastomers is developed to reduce computation time. The domain of bistability is investigated taking into account the combined effect of prestrain orientation and the ratio of prestrains, laminate size, and aspect ratio. Modeling of snap-through actuation requirements shows that actuation effort is maximum when one of the prestressed laminae is on a diagonal and the angle between prestrains is 45°.

1. Introduction

Bistable laminates are attractive for morphing structures and energy harvesting applications as they can exhibit two deformed stable shapes and require actuation only to switch between the shapes [1]. Bistability is typically achieved by incorporating elastic [2] or plastic [3] residual stress in the structure. The most widely studied form of bistability is based on thermally-induced residual stress in fiber-reinforced polymeric (FRP) laminates [4]. Other methods for incorporating elastic residual stress include fiber-prestressing [5], viscoelastic prestress [6], and mechanical prestress [7].

Hyer [4] was the first to study the room-temperature shapes of thin asymmetric FRP laminates. Subsequently, discrepancies in models based on classical laminate theory were addressed with a new model that included geometric nonlinearity (per von Karman's hypothesis) [8]. The analytical model was further developed with assumptions on displacement polynomials [9], methods to calculate shear strains [10], and inclusion of actuation forces [11]. The stable shapes of FRP laminates are a function of the laminates' size, shape, and material properties. The existence of two stable shapes is a function of the length-to-thickness ratio of the laminates [12–14].

On the topic of bistable FRP laminates, significant attention has been devoted to $0_2/90_2$ or "cross-ply" laminates due to symmetry in the cylindrical stable shapes and sharp shape-transition when actuated. Other types of ply orientations studied include an arbitrary angle θ such as $\theta_2/(90+\theta)_2$, $0_2/90_2/\theta_2$, and $0_2/\theta_2$; the subscript in θ_n denotes the number of plies. Hyer [4] and Jun and Hong [15] showed that $0_2/90_2/\theta_2$ laminates are not bistable. Most $0_2/\theta_2$ laminates exhibit only one curvature. On the other hand, $\theta_2/(90+\theta)_2$ laminates exhibit bistable cylindrical curvatures that are twisted relative to the global coordinate system [16], but are limited by the small range of possible shapes; the shapes are all cylindrical and differ only in orientation. Betts et al. [17] experimentally characterized the shapes of a family of $\theta_2/(90+\theta)_2$ laminates.

Overall, there are few studies on bistability arising from fully arbitrary ply orientations, i.e., $0_2/\theta_2$. FRP laminates offer a limited range of bistable curvatures due to inherent limitations; only thin laminates exhibit bistability, plies should be symmetric with respect to the geometric mid-plane, and thermally-induced residual stress is a global parameter rather than local. These limitations can be addressed by switching from thermally-induced residual stress to mechanical prestress. Chillara and Dapino [7] developed bistable laminates that comprise two mechanically-prestressed elastomeric matrix composites (EMC [18,19]) on either face of an isotropic core layer. These

* Corresponding author.
E-mail addresses: chillara.1@osu.edu (V.S.C. Chillara), dapino.1@osu.edu (M.J. Dapino).

https://doi.org/10.1016/j.compstruct.2019.111502
Received 17 June 2019; Received in revised form 2 August 2019; Accepted 23 September 2019
Available online 24 September 2019
0263-8223/

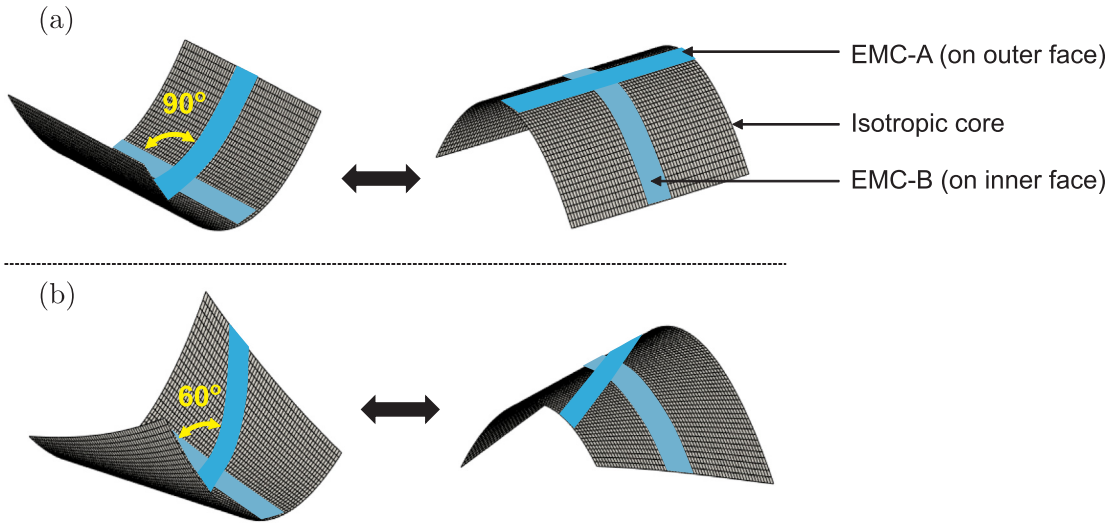

Fig. 1. Mechanically-prestressed bistable laminate with (a) orthogonal EMCs and (b) non-orthogonal EMCs.

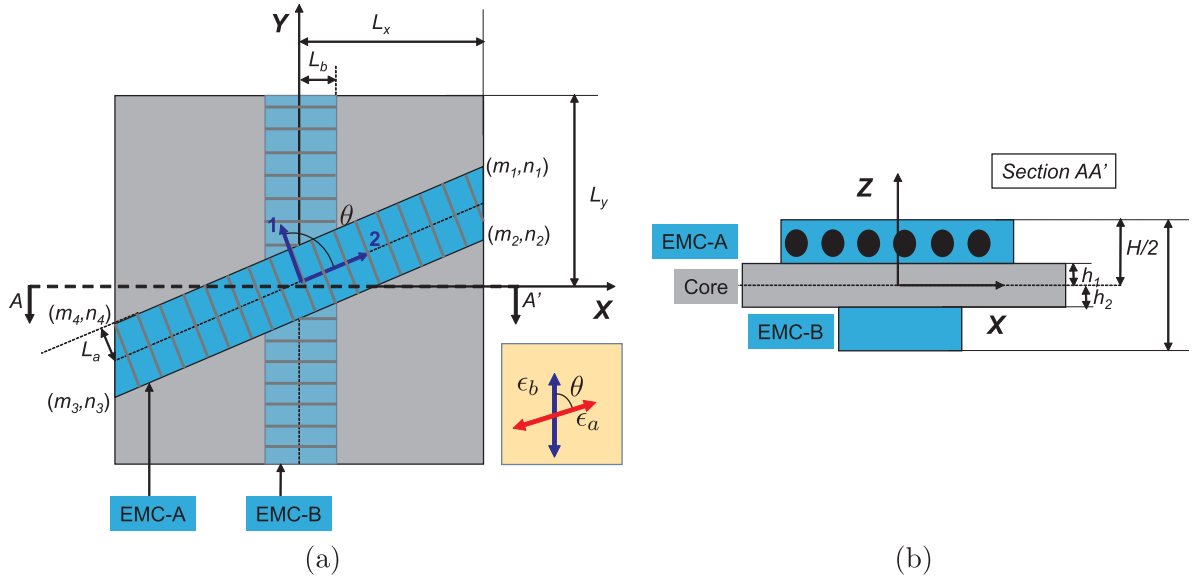

Fig. 2. Schematic representation of a mechanically-prestressed bistable laminate in (a) top view and (b) sectional view.

composites have two sources of locally-applied residual stress and therefore have a broader design space for bistable curvatures.

The EMCs in a mechanically-prestressed laminate are reinforced with fibers along their width, enabling near-zero in-plane Poisson's ratio when prestressed. When the EMCs are orthogonal to each other, the laminate exhibits orthogonal cylindrical shapes that are weakly coupled; the magnitude of each curvature can be varied by changing the prestrain in the EMC on the concave face. The permissible range of EMC prestrains is defined by a critical prestrain ratio. Beyond the critical ratio, the composite has a single curved shape. Phenomena related to shape bifurcation, such as the domain of bistability and snap-through actuation forces, have been studied in laminates with orthogonal EMCs using high-order displacement polynomials [20]. These phenomena however, are also influenced by the orientation of the EMCs relative to each other and to the structure's geometry.

This paper presents mechanically-prestressed bistable laminates with non-orthogonal EMCs. An example of such a laminate is shown in Fig. 1(b) alongside one with orthogonal prestressed EMCs (Fig. 1(a)). Prior work by Chillara and Dapino [7] on laminates with orthogonal EMCs has shown that the weakly-coupled cylindrical shapes can be calculated using the assumption of constant curvature. This assumption is insufficient for modeling laminates with non-orthogonal EMCs because their shapes are expected to be non-cylindrical and contain twist that is not constant across the laminate. The spatial variation in curvatures in non-orthogonal EMC configurations is a result of a coupling between shapes such that each shape is influenced by both sources of EMC prestress. Therefore, existing analytical models are insufficient and an advanced model based on higher order polynomials is required to analyze bistable laminates with arbitrary orientations of mechanical prestress. The model developed in this work is a generalization of the model presented in [7] and the two models are equivalent when the EMCs are orthogonal.

The remaining sections in this paper are organized as follows: an analytical laminated-plate model for laminates with non-orthogonal prestress is developed in Section 2; in Section 3, a fabrication process that improves upon existing methods for mechanically-prestressed bistable laminates is presented and the model is validated against the shapes of the composites prepared; laminates shapes are calculated in various EMC orientations and the effect of orientation on the coupling of shapes is discussed in Section 4. A sensitivity study is conducted in Section 5 to investigate the combined effect of EMC orientation and a variety of parameters including EMC-prestrain ratio, laminate size,

Table 1
Coordinates of an EMC-A oriented at angle θ with respect to the Y axis.

Point	0 to $\pi/4$	$\pi/4$ to $\pi/2$
(m_1, n_1)	$(L_y\tan\theta - L_a\sec\theta, L_y)$	$(L_x, L_x\cot\theta + L_a\csc\theta)$
(m_2, n_2)	$(L_y\tan\theta + L_a\sec\theta, L_y)$	$(L_x, L_x\cot\theta - L_a\csc\theta)$
(m_3, n_3)	$(-L_y\tan\theta + L_a\sec\theta, -L_y)$	$(-L_x, -L_x\cot\theta - L_a\csc\theta)$
(m_4, n_4)	$(-L_y\tan\theta - L_a\sec\theta, -L_y)$	$(-L_x, -L_x\cot\theta + L_a\csc\theta)$

aspect ratio, and actuation pressure, on bistability.

2. Analytical model

The purpose of the analytical model is to calculate the stable shapes of a bistable laminate that has prestressed EMCs at non-orthogonal angles (Fig. 2). A rectangular planform is considered in the analysis. The EMCs on the top and bottom faces are referred to as EMC-A and EMC-B, respectively. Throughout this paper, the orientation of EMC-B is considered to be fixed and prestrain is applied to it along the Y axis. On the other hand, EMC-A is positioned and prestressed at an angle relative to the prestrain direction in EMC-B. The angle between prestrain directions in the EMCs is denoted by θ. The complete range of unique shapes can be obtained by sweeping θ from 0° to 90°. The vertices of the rotated EMC-A, calculated using rotation matrices, are listed in Table 1.

The composite is modeled as a laminated plate based on classical laminate theory in conjunction with von Karman's hypothesis [21]. Plane-stress and plane-strain conditions are assumed. In-plane strains and the out-of-plane deflection are approximated using unknown polynomial functions. To account for non-constant curvature and twist due to non-orthogonal prestrain orientations, the in-plane strains and out-of-plane deflection of the laminate are described using fourth order polynomials. Higher order polynomials have been used for modeling stable shapes under the influence of elastic boundary conditions [22,23], asymmetric planform shapes [24,25], and calculation of snap-through loads [26,27,20]. Strain energy of the laminate is calculated in terms of the unknown polynomial functions. Stable shapes are obtained by minimizing the strain energy with respect to the unknown coefficients. The resulting nonlinear equations are solved using the Newton-Raphson method. In this work, the in-plane strains and the out-of-plane deflection are assumed to be fourth order polynomials in order to calculate shapes with non-uniform curvatures resulting from non-orthogonal prestrains. When the EMCs are orthogonal, second order polynomials are accurate for shape calculation.

2.1. Strain model

Strain of an arbitrary point (x, y, z) on a composite plate is written in terms of its displacements (u, v, w) as:

$$\epsilon_x = \frac{\partial u}{\partial x} + \frac{1}{2}\left(\frac{\partial w}{\partial x}\right)^2, \tag{1}$$

$$\gamma_{xy} = \frac{\partial u}{\partial y} + \frac{\partial v}{\partial x} + \frac{\partial w}{\partial x}\frac{\partial w}{\partial y}, \tag{2}$$

$$\epsilon_y = \frac{\partial v}{\partial y} + \frac{1}{2}\left(\frac{\partial w}{\partial y}\right)^2. \tag{3}$$

Displacements of the composite can be expressed in terms of the displacement of its mid-plane (u_0, v_0, w_0) as:

$$u\left(x, y, z\right) = u_0(x) - z\frac{\partial w_0}{\partial x}, \tag{4}$$

$$v\left(x, y, z\right) = v_0(y) - z\frac{\partial w_0}{\partial y}, \tag{5}$$

$$w(x, y, z) = w_0(x, y). \tag{6}$$

Strains of the composite can be expressed in terms of its mid-plane displacements by substituting (4)–(6) into (1)–(3):

$$\epsilon_x = \frac{\partial u_0}{\partial x} + \frac{1}{2}\left(\frac{\partial w_0}{\partial x}\right)^2 - z\left(\frac{\partial^2 w_0}{\partial x^2}\right), \tag{7}$$

$$\gamma_{xy} = \frac{\partial u_0}{\partial y} + \frac{\partial v_0}{\partial x} + \frac{\partial w_0}{\partial x}\frac{\partial w_0}{\partial y} - 2z\left(\frac{\partial^2 w_0}{\partial y \partial x}\right), \tag{8}$$

$$\epsilon_y = \frac{\partial v_0}{\partial y} + \frac{1}{2}\left(\frac{\partial w_0}{\partial y}\right)^2 - z\left(\frac{\partial^2 w_0}{\partial y^2}\right), \tag{9}$$

yielding the relations:

$$\epsilon_x = \epsilon_x^0 + z\kappa_x^0, \qquad \gamma_{xy} = \gamma_{xy}^0 + z\kappa_{xy}^0, \qquad \epsilon_y = \epsilon_y^0 + z\kappa_y^0, \tag{10}$$

where ϵ_x^0 and ϵ_y^0 are the in-plane axial strains, γ_{xy}^0 is the in-plane shear strain, and κ_x^0, κ_y^0, and κ_{xy}^0 are the curvatures and twist, respectively, of the geometric mid-plane.

The out-of-plane deflection w_0 (Z direction) is approximated as a fourth order polynomial whose coefficients only have even powers,

$$w_0(x, y) = k_{20}x^2 + k_{11}xy + k_{02}y^2 + k_{40}x^4 + k_{31}x^3y + k_{22}x^2y^2 + k_{13}xy^3 + k_{04}y^4. \tag{11}$$

The choice of terms is valid because each shape of the composite is expected to be a combination of cylindrical curvature components. Hyer [8] showed that in-plane strains ϵ_x^0, ϵ_y^0 can be approximated using polynomials with even degree terms. Based on this assumption, fourth order polynomials are chosen for ϵ_x and ϵ_y as:

$$\epsilon_x^0 = c_{00} + c_{20}x^2 + c_{11}xy + c_{02}y^2 + c_{40}x^4 + c_{31}x^3y + c_{22}x^2y^2 + c_{13}xy^3 + c_{04}y^4, \tag{12}$$

$$\epsilon_y^0 = d_{00} + d_{20}x^2 + d_{11}xy + d_{02}y^2 + d_{40}x^4 + d_{31}x^3y + d_{22}x^2y^2 + d_{13}xy^3 + d_{04}y^4. \tag{13}$$

Displacements of the mid-plane ($z = 0$) are obtained by integrating (1) and (3) as:

$$\begin{aligned} u_0(x, y) = {} & c_{00}x + f_1y + \frac{c_{20} - 2k_{20}^2}{3}x^3 + \frac{c_{11} - 2k_{11}k_{20}}{2}x^2y + \frac{2c_{02} - k_{11}^2}{2}xy^2 \\ & + f_2y^3 + \frac{c_{40} - 8k_{20}k_{40}}{5}x^5 + \frac{c_{31} - 4k_{11}k_{40} - 6k_{20}k_{31}}{4}x^4y \\ & + \frac{c_{22} - 3k_{11}k_{31} - 4k_{20}k_{22}}{3}x^3y^2 + \frac{c_{13} - 2k_{11}k_{22} - 2k_{13}k_{20}}{2}x^2y^3 \\ & + (c_{04} - k_{11}k_{13})xy^4 + f_3y^5, \end{aligned} \tag{14}$$

$$\begin{aligned} v_0(x, y) = {} & d_{00}y + f_1x + \frac{(d_{02} - 2k_{02}^2)}{3}y^3 + \frac{(d_{11} - 2k_{11}k_{02})}{2}xy^2 + \frac{(2d_{20} - k_{11}^2)}{2}x^2y \\ & + f_4x^3 + \frac{d_{04} - 8k_{02}k_{04}}{5}y^5 + \frac{(d_{13} - 4k_{11}k_{04} - 6k_{02}k_{13})}{4}y^4x \\ & + \frac{(d_{22} - 3k_{11}k_{13} - 4k_{02}k_{22})}{3}y^3x^2 + \frac{(d_{31} - 2k_{11}k_{22} - 2k_{31}k_{02})}{2}y^2x^3 \\ & + (d_{40} - k_{11}k_{31})yx^4 + f_5x^5. \end{aligned} \tag{15}$$

Shear strain γ_{xy} is calculated by substituting (11), (14), and (15) in (8).

Given that the EMCs are anisotropic, strains in the material should be expressed in terms of the laminate's strain. EMC-B is aligned such that its material-coordinate axes coincide with the laminate's coordinate axes. For EMC-A however, strains are expressed in material coordinates as:

$$\begin{Bmatrix} \epsilon_1 \\ \epsilon_2 \\ \epsilon_6 \end{Bmatrix} = \begin{bmatrix} \cos^2\theta & \sin^2\theta & \sin\theta\cos\theta \\ \sin^2\theta & \cos^2\theta & -\sin\theta\cos\theta \\ -2\sin\theta\cos\theta & 2\sin\theta\cos\theta & \cos^2\theta - \sin^2\theta \end{bmatrix} \begin{Bmatrix} \epsilon_x \\ \epsilon_y \\ \gamma_{xy} \end{Bmatrix}. \tag{16}$$

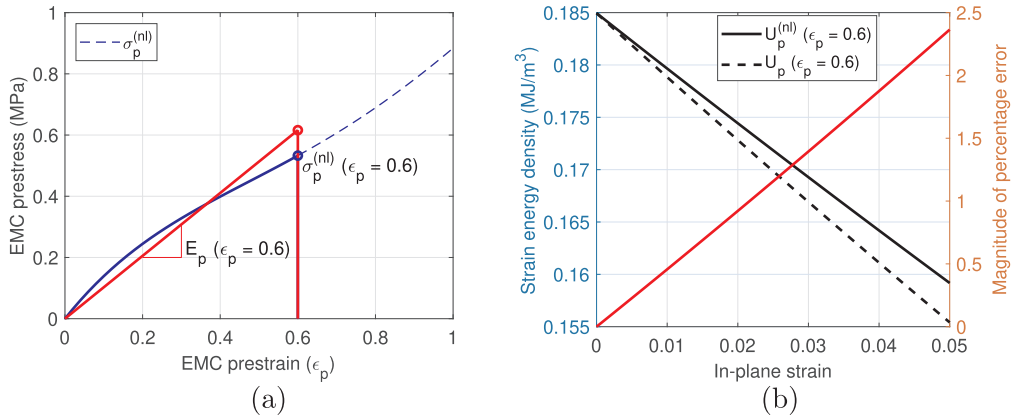

Fig. 3. (a) Stress-strain curve of an EMC that is reinforced with fibers in the 1-direction and stretched in the 2-direction; (b) error in the calculation of strain energy density using the linear-equivalent EMC constitutive expression relative to the nonlinear expression.

2.2. Linear-equivalent constitutive relations for prestressed EMCs

In previous works on mechanically-prestressed bistable composites [7], the EMCs' constitutive material response in the prestrained direction was described using the following experimentally-obtained expression:

$$\sigma_p^{(nl)} = -0.698\ \epsilon_p^4 + 2.29\ \epsilon_p^3 - 2.306\ \epsilon_p^2 + 1.598\ \epsilon_p \quad [\text{MPa}], \tag{17}$$

where $\sigma_p^{(nl)}$ is the prestress due to an applied prestrain ϵ_p in the EMC; shown with a blue dashed line in Fig. 3(a). The EMC's strain energy for a given ϵ_p was computed as the area under the stress-strain curve and written in terms of composite strains as:

$$U_p^{(nl)} = \int_V \left[\frac{-0.698}{5}(\epsilon_p - \epsilon)^5 + \frac{2.29}{4}(\epsilon_p - \epsilon)^4 - \frac{2.306}{3}(\epsilon_p - \epsilon)^3 + \frac{1.598}{2}(\epsilon_p - \epsilon)^2\right] dV, \tag{18}$$

where ϵ is a component of the composite's in-plane strain. While a bi-quadratic constitutive expression is accurate for describing the composites' mechanics, there is a tradeoff in computational cost when it is paired with high-order displacement polynomials and rotation matrices in the strain model. In this paper, we present a linear-equivalent EMC model based on a point-wise elastic modulus. At each prestrain, the area under the nonlinear stress-strain curve is equated to a constitutive expression based on Hooke's law. The point-wise modulus E_p, shown in Fig. 3(a), is then calculated as:

$$E_p = \frac{2}{\epsilon_p^2}\int_0^{\epsilon_p} \sigma_p^{(nl)} d\,\epsilon_p. \tag{19}$$

Based on E_p, strain energy U_p in the prestressed direction in an EMC layer within the composite is calculated as:

$$U_p = \int_V \frac{1}{2} E_p(\epsilon_p - \epsilon)^2 dV. \tag{20}$$

The assumption in the linear-equivalent model is that the point-wise modulus is a function only of the applied prestrain and is invariant to strains in the composite. In practice, in-plane strains in bistable composites are only as high as 5–6%. At 60% EMC prestrain, the error in in-plane strain in the linear-equivalent model is calculated to be 2.35% (Fig. 3(b)). This minimal error is an acceptable tradeoff and therefore the linear model is used to achieve faster computation.

2.3. Strain energy computation

The strain energy (U_c) of the core is expressed in terms of its material properties and dimensions as:

$$U_c = \int_{-L_x}^{L_x}\int_{-L_y}^{L_y}\int_{h_2}^{h_1}\left(\frac{1}{2}\overline{Q}_{11}\,\epsilon_x^2 + \overline{Q}_{12}\,\epsilon_x\epsilon_y + \frac{1}{2}\overline{Q}_{22}\,\epsilon_y^2 + \frac{1}{2}\overline{Q}_{16}\gamma_{xy}\,\epsilon_x + \frac{1}{2}\overline{Q}_{26}\gamma_{xy}\,\epsilon_y + \frac{1}{2}\overline{Q}_{66}\gamma_{xy}^2\right) dz dy dx, \tag{21}$$

where $\overline{Q}_{ij}$ (i = 1, 2, 6) are the plane-stress reduced stiffnesses of the composite [28]. Strain energy (U_b) of EMC-B is written as:

$$U_b = \int_{-L_b}^{L_b}\int_{-L_y}^{L_y}\int_{-H/2}^{h_2}\left(\frac{1}{2}\overline{Q}_{11}\,\epsilon_x^2 + \frac{1}{2}\overline{Q}_{22}^p(\epsilon_b - \epsilon_y)^2 + \frac{1}{2}\overline{Q}_{66}\gamma_{xy}^2\right) dz dy dx. \tag{22}$$

Note that the coefficients $\overline{Q}_{12}$, $\overline{Q}_{16}$, $\overline{Q}_{26}$ are zero as the EMC's in-plane Poisson's ratio is assumed to be zero. The strain energy integrand for EMC-A is written in terms of its material coordinates (see (16)) as:

$$dU_a\Big(x, y\Big) = \int_{h_1}^{H/2}\left(\frac{1}{2}\overline{Q}_{11}\,\epsilon_1^2 + \frac{1}{2}\overline{Q}_{22}^p(\epsilon_a - \epsilon_2)^2 + \frac{1}{2}\overline{Q}_{66}\gamma_6^2\right) dz. \tag{23}$$

The integral and its limits for EMC-A for various ranges of prestrain

Table 2
Limits of integration for the computation of strain energy of EMC-A.

θ	Integral
$\left\{0, \frac{\pi}{4}\right\}$	$U_a = \int_{-L_x}^{L_x}\left(\int_{n_3}^{n_1} dU_a dy - \int_{\frac{n_4-n_1}{m_4-m_1}\left(x+L_x\right)+n_4}^{n_1} dU_a dy - \int_{n_3}^{\frac{n_2-n_3}{m_2-m_3}\left(x-L_x\right)+n_2} dU_a dy\right) dx$
$\left\{\frac{\pi}{4}, \frac{\pi}{2}\right\}$	$U_a = \int_{-L_y}^{L_y}\left(\int_{m_4}^{m_2} dU_a dx - \int_{m_4}^{\frac{m_4-m_1}{n_4-n_1}\left(y+L_y\right)+m_4} dU_a dx - \int_{\frac{m_2-m_3}{n_2-n_3}\left(y+L_y\right)+m_3}^{m_2} dU_a dx\right) dy$

orientation θ are listed in Table 2.

2.4. Work done by actuation pressure

To quantify the snap-through actuation loads as a function of prestrain orientation, a uniformly distributed transverse pressure (P) is applied in the ±Z direction. The corresponding work done on the composite is written as:

$$W = \int_{-Lx}^{Lx} \int_{-Ly}^{Ly} P.\, w_0 \mathrm{d}y\mathrm{d}x. \tag{24}$$

2.5. Computation of composite shape

The composite's stable shapes are calculated by minimizing the net energy using the Rayleigh-Ritz method:

$$\sum_i \frac{\partial(U_a + U_b + U_c - W)}{\partial C_i} = 0, \tag{25}$$

where C_i is the set of coefficients c, d, and k from (12), (13), and (6), respectively. The expressions for strain energy and actuation work are derived using the MAPLE symbolic solver. Partial derivatives with respect to the 31 coefficients are obtained and the resulting nonlinear equations are solved using the Newton-Raphson method (in MATLAB).

3. Composite fabrication and model validation

Composites with four prestrain orientations, i.e., θ = 30°, 45°, 60°, and 90° are fabricated to demonstrate bistability and validate the analytical model. The fabrication process for the EMCs and the bistable composites were presented by Chillara and Dapino [7]. In previous works, prestressed layers were laminated in a two stage process. In this work a method for single-stage fabrication is presented (Fig. 4). EMCs of dimensions 15.2 × 15.2 × 2 mm are stretched to a prestrain of 0.4 (40%) and held onto a base plate using clamps. A spring steel plate of dimensions 76.2 × 76.2 × 0.076 mm is inserted between the EMCs and laminated by applying a flexible silcone adhesive (DAP Automarine silicone sealant). Weights are placed on the composite to keep the bonded regions under pressure during the 24-h curing process. The stable shapes of the manufactured specimens are shown in Fig. 5.

The composites' material properties, measured using tensile tests, are listed in Table 3. Using the same material properties, dimensions, and prestress as in the manufactured composites, the stable shapes are calculated using the analytical model as a function of prestrain orientation. The measured and calculated out-of-plane deflections at all vertices are compared as shown in Fig. 6. Note that vertices on a diagonal have equal deflections. In the manufactured samples, deflection is calculated as the average of vertex deflections on each diagonal. The measured deflections are in agreement with the calculated shapes, thereby rendering the model valid. The maximum error between the calculated and measured shapes is 10.8%, 7.7%, 11%, and 3% for θ = 30°, 45°, 60°, and 90°, respectively. The dependence of stable shapes on prestrain orientation is discussed in Section 4.

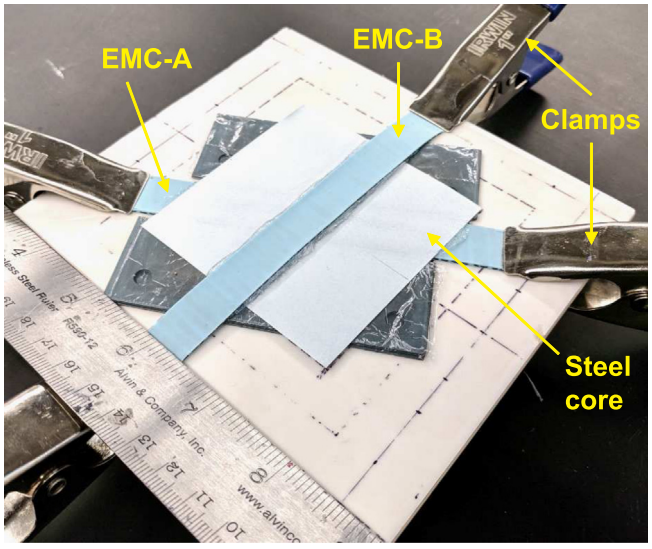

Fig. 4. Fabrication setup for a mechanically-prestressed bistable composite.

4. Calculation of stable shapes

The composite is shown to have two stable shapes for various values of θ as shown in Fig. 7. To study the effect of material and geometric parameters, the shapes are represented using deflection at the vertices. Fig. 8 shows the two stable shapes plotted for $\epsilon_a \triangleq \epsilon_b = 0.6$. At $\theta = 0$, the EMCs are parallel to each other. Application of a prestrain yields no flexure in the composite as the bending forces cancel out. However, there exists a compressive stress in the core layer that could be harnessed to tailor buckling/crumpling of the core. At non-zero prestrain angles, the composite exhibits two stable shapes in response to equal prestrains applied to the EMCs.

The dominant deformation mode is twist rather than pure-bending since deflection in the second stable shape is observed at the adjacent vertex. Further, twist is not constant across the composite given that w_0 at a given θ is not equal in magnitude in both shapes (Fig. 8). Therefore, the assumption of constant curvature and twist is insufficient to calculate the shapes resulting from non-orthogonal prestress configurations. As a consequence, fourth order polynomials for in-plane strains and deflection are the minimum polynomials that accurately describe the stable shapes.

As θ tends to 90°, deflection at all vertices converges to the same magnitude, indicating that the shapes are cylindrical. To demonstrate weak coupling of the shapes at θ = 90°, prestrain in EMC-A is reduced to 0.54. Results show that at angles other than 90°, deflections in both shapes are affected by the change in prestrain. At 90°, only the upward curvature is affected by the change in ϵ_a.

5. Sensitivity study

5.1. Effect of EMC prestrain

In mechanically-prestressed composites with two sources of residual stress, there exists a critical (minimum) ratio of EMC prestrains for the composite to be bistable [20]. In other words, when prestrain in one EMC is sufficiently low relative to prestrain in the other EMC, the compsite has only one stable shape. In the case of orthogonal EMCs, only one cylindrical shape exists and its magnitude is primarily influenced by the higher EMC prestrain. For configurations with non-orthogonal prestressed EMCs, the critical prestrain is expected to depend on the prestrain orientation based on the fact that the shapes are not weakly coupled.

Fig. 9 shows deflection w_0 at (L_x, L_y) in both shapes as a function of θ for prestrain ϵ_a ranging from 0.04 to 0.6. Prestrain ϵ_b is maintained constant at 0.6. The solid and dotted lines represent the bistable and monostable regimes, respectively. For θ: 45° → 90°, the minimum ϵ_a for bistability is calculated to be 0.14. As θ is reduced below 45°, the critical ϵ_a increases with a decrease in θ. Fig. 10 shows a second scenario where prestrains $\epsilon_a = 0.6$ and $0.04 \leqslant \epsilon_b \leqslant 0.6$. Below a critical $\epsilon_b$of 0.38, the composite exhibits a monostable positive curvature whereas above 0.38, it is bistable up to θ = 45°. Beyond θ = 45°, the critical prestrain increases with an increase in θ. Based on the two scenarios, we see that critical prestrain for bistability is higher in the EMC that is parallel to a laminate's edge; such an EMC has minimum length and therefore minimal strain energy when prestressed. In both cases, bandwidth of usable prestrain is maximum and minimum when the EMCs are

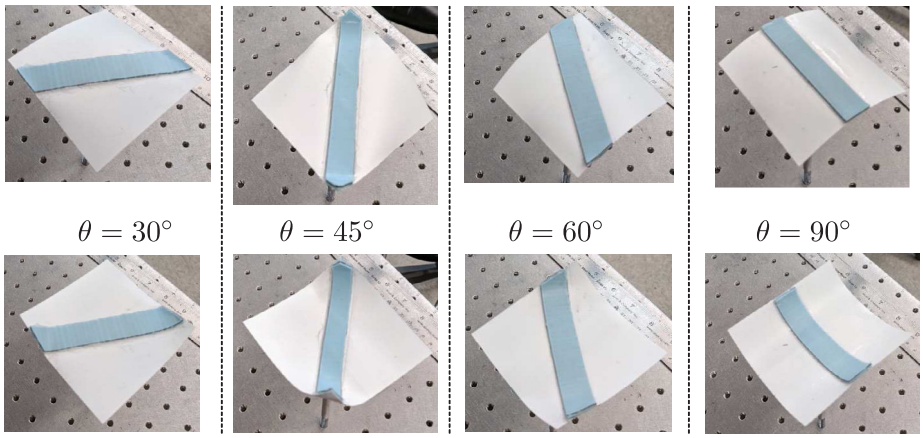

Fig. 5. Stable shapes of the composites prepared. Areal dimensions are 76.2 × 76.2 mm.

Table 3
Measured material properties of the laminae of modeled and tested prestressed laminates. Note: E_1 and G_{12} are modified values per the assumptions discussed in [7].

Lamina	E_1 (MPa)	E_2 (MPa)	G_{12} (MPa)	ν_{12}	ν_{21}
EMC	0.4	Point-wise	1.2	0	0
Core (steel)	200,000	200,000	78,125	0.28	0.28

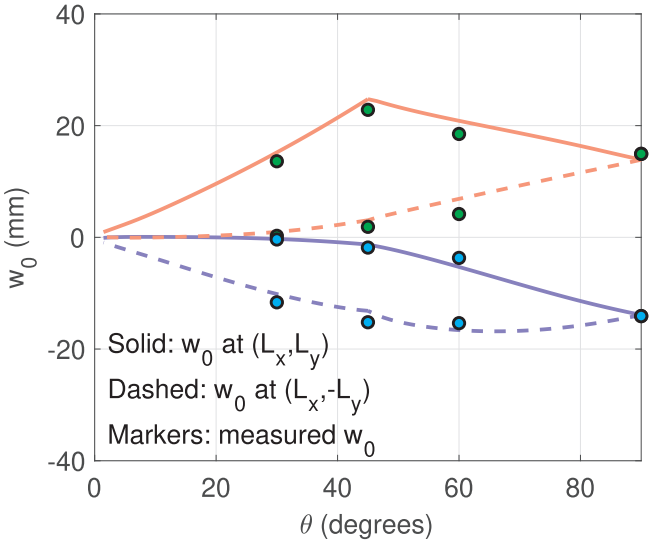

Fig. 6. Out-of-plane deflection at the vertices of the laminate obtained through modeling and experiments.

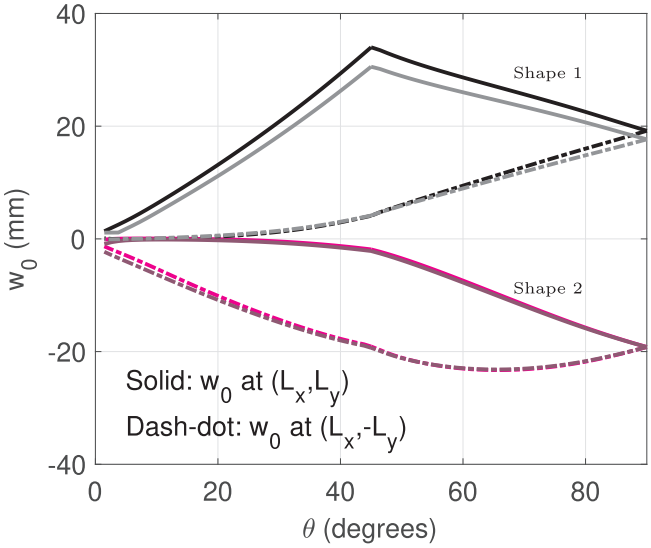

Fig. 8. Out-of-plane displacement of vertex at (L_x, L_y). The black-magenta set represent the case of $\epsilon_a \triangleq \epsilon_b = 0.6$. The gray-purple set represent the case of $\epsilon_a = 0.54$, $\epsilon_b = 0.6$.

orthogonal and parallel, respectively.

5.2. Effect of laminate size

The deflections of square composites calculated for various sizes are shown in Fig. 11. Sizes are expressed in terms of reference areal dimensions of 76.2 × 76.2 mm and a magnification factor *M*; thickness of the core is constant at 0.076 mm. EMC width and prestrain are

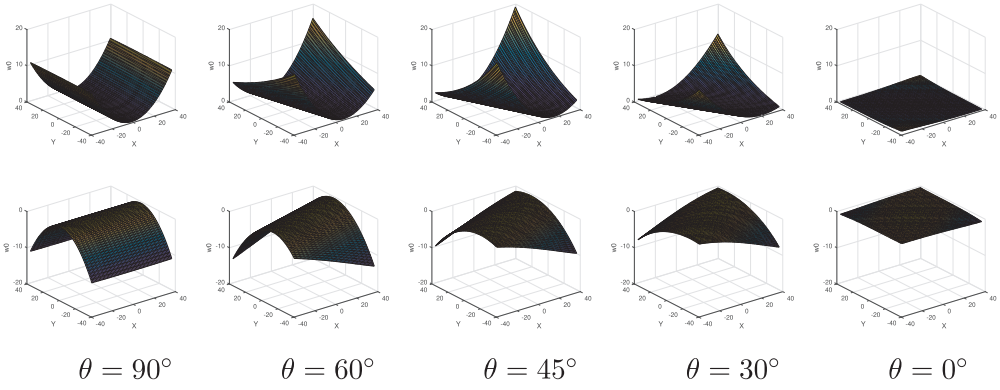

Fig. 7. Calculated stable shapes for various EMC orientations in a bistable laminate.

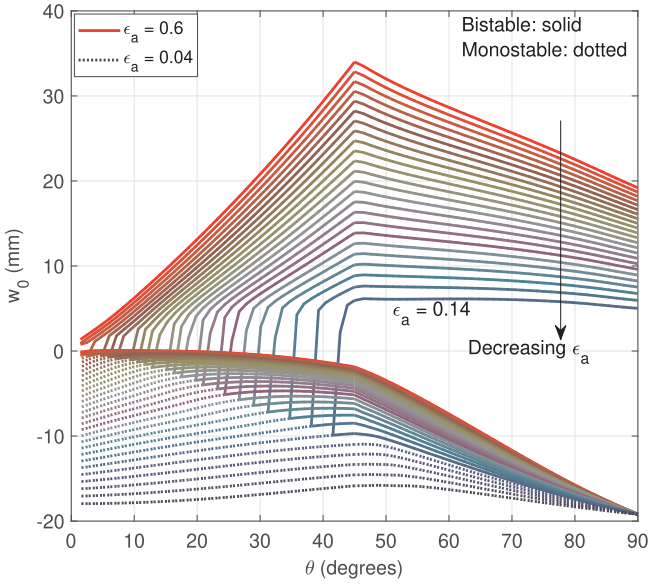

Fig. 9. Out-of-plane displacement of vertex at (L_x, L_y) for $\epsilon_b = 0.6$ and ϵ_a ranging from 0.04 to 0.6.

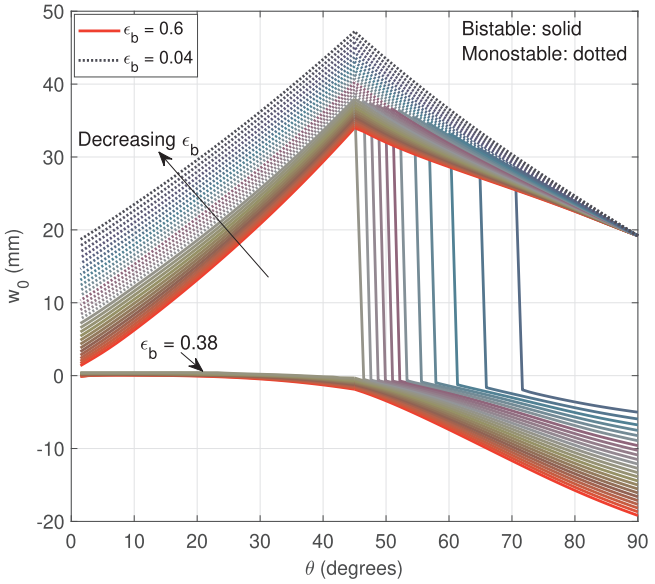

Fig. 10. Out-of-plane displacement of vertex at (L_x, L_y) for $\epsilon_a = 0.6$ and ϵ_b ranging from 0.04 to 0.6.

maintained constant at 15.2 mm and 0.6, respectively. Deflection of the vertex is found to increase with increase in M. This magnification in the deformed shapes is independent of θ. Notably, bistability is maintained at smaller sizes; $M = 0.5$ corresponds to 38.1×38.1 mm. This result however, is due to the appropriate choice of core modulus, thickness, and EMC prestrains. Chillara and Dapino [7] showed that with softer core materials, there exists a critical size below which the composite has a single saddle shape. This analysis shows that bistability created using mechanical prestressed laminae is highly scalable.

5.3. Effect of aspect ratio

Aspect ratio is defined as the ratio of the lengths of the longer edge to the shorter edge in a rectangular composite. By definition, AR is greater than 1 and is used as a multiple on either L_x or L_y similar to the multiple M in Section 5.2. In the first study, rectangular composites with the longer edges along the X axis are studied. Deflections are

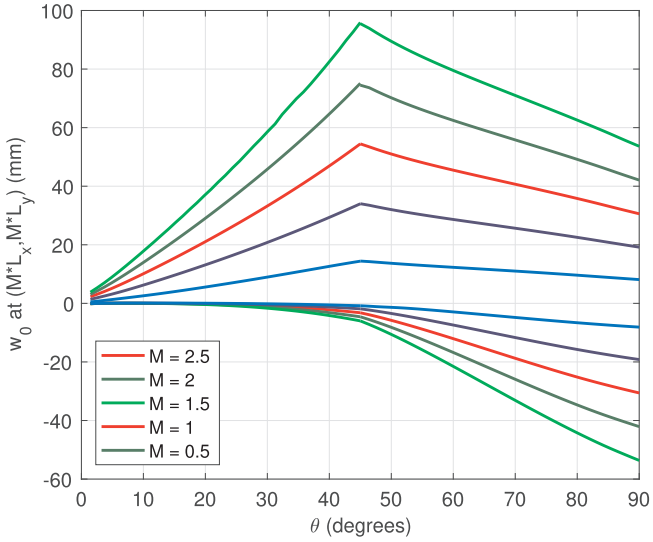

Fig. 11. Out-of-plane displacement of vertex at (L_x, L_y) for various laminate sizes. Width of the EMCs is maintained constant at 15.24 mm. $\epsilon_a \triangleq \epsilon_b = 0.6$.

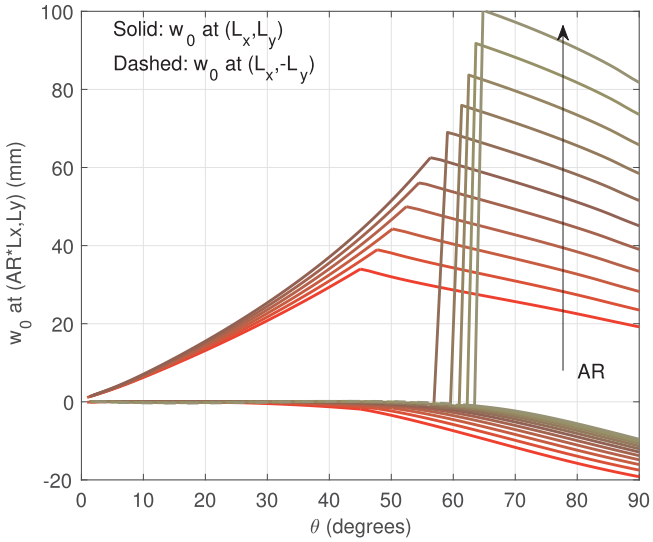

Fig. 12. Out-of-plane displacement of vertex at $(AR * L_x, L_y)$. Width of the EMCs is maintained constant at 15.24 mm. $\epsilon_a \triangleq \epsilon_b = 0.6$.

calculated at the vertex $(AR * L_x, L_y)$ for AR ranging from 1 to 2 and $L_x \triangleq L_y = 76.2$ mm (Fig. 12). For square laminates ($AR = 1$), the maximum positive deflection occurs at $\theta = 45°$. This deflection peak shifts away from 45° to a higher value as the aspect ratio increases, indicating that deflection is maximum when the prestressed EMC-A is oriented along the diagonal of a rectangular composite. With increase in AR, shape 1 (positive w_0) is amplified and shape 2 is reduced for all values of θ. At a critical AR of 1.6, shape 1 does not exist below a critical θ and the composite is monostable in shape 2.

In another study, the longer edge of the rectangular composites is along the Y axis. For the same range of AR and areal dimensions as in the first study, deflections are calculated at $(L_x, AR * L_y)$ (Fig. 13). With increase in AR, shape 2 is magnified whereas shape 1 is diminished. The peak value of deflection in shape 1 remains nearly constant with increase in AR and it corresponds to the orientation where prestress in EMC-A is along the diagonal. Beyond a critical AR of 1.5, the composite is monostable in orientations where both EMCs terminate on the same edge ($y = \pm L_y$). Based on the two studies, allowable aspect ratio for bistability is a function of prestrain orientation. In both cases, the composite is monostable in shape 2 outside the domain of bistability.

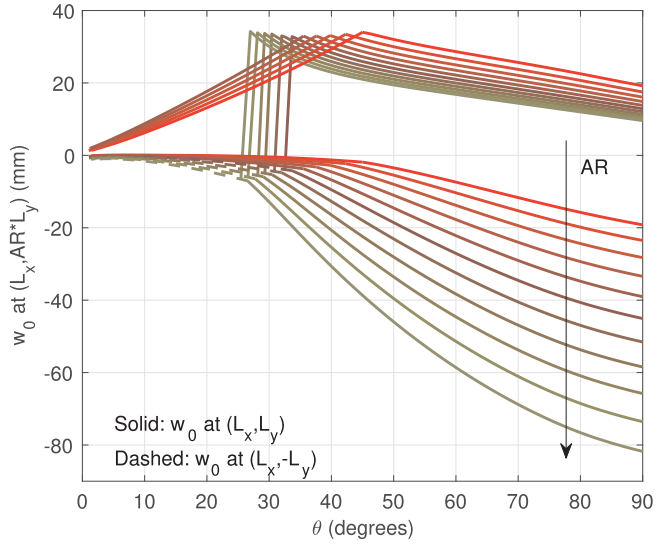

Fig. 13. Out-of-plane displacement of vertex at $(L_x, AR * L_y)$. Width of the EMCs is maintained constant at 15.24 mm. $\epsilon_a \triangleq \epsilon_b = 0.6$.

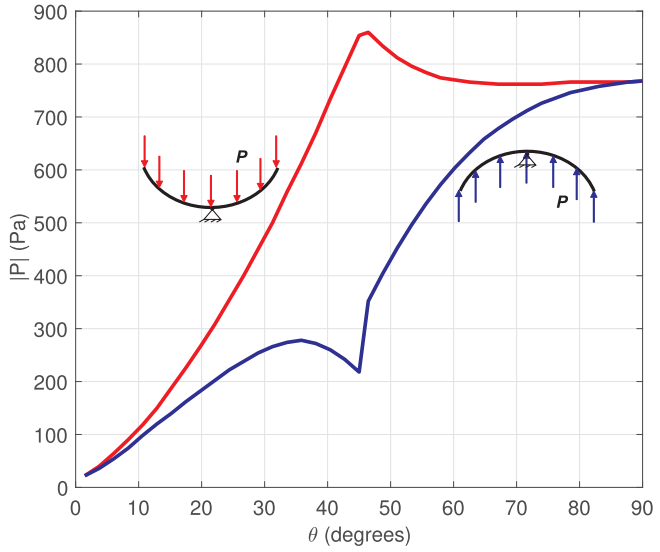

Fig. 14. Snap-through actuation pressure as a function of prestrain orientation.

5.4. Actuation requirements

The effect of prestrain orientation on the forces required for snap-through between stable shapes is studied in this section. A uniformly distributed pressure load P acting in the $\pm Z$ direction is chosen for this analysis; point loads at the vertices are not ideal for comparison because the vertices do not deform to the same extent in both shapes over the complete range of θ. Stable shapes are calculated over a range of pressure values and the pressure required for snap-through is identified as the point of discontinuity in the force-deflection curve. Snap-through pressures for various values of θ are plotted in Fig. 14. The analysis is done on square composites of areal dimensions 76.2 × 76.2 mm.

Actuation pressure is found to be higher in shape 1 than in shape 2 for all values of θ except 0° and 90°. In shape 1 actuation pressure increases with increase in θ and reaches a maximum at 45°. In contrast, actuation pressure in shape 2 has a local minima at 45°. In bistable composites, the potential energy minima corresponding to stable shapes are separated by a local maxima that should be overcome to achieve snap-through. The increasing trend in actuation pressure can be explained by the increasing separation between the potential energy minima between stable shapes; at $\theta = 0^{\circ}$ the structure has neither bistability nor curvature, whereas at $\theta = 90°$ it is bistable with cylindrical curved shapes. Peak values are observed at the 45° point because the deflections are maximum in this orientation; EMC-A has maximum length in the 45° orientation and therefore the input strain energy is maximum for a given EMC prestrain.

6. Concluding remarks

Bistable laminates with non-cylindrical curved shapes arising from elastic residual stress have been investigated for the first time through this work. Mechanically-prestressed elastomeric laminae configured at non-orthogonal angles yield a range of bistable shapes that include non-constant curvature and twist in the laminate. Non-cylindrical stable shapes are influenced by prestrain in both the EMCs whereas cylindrical shapes resulting from orthogonal EMCs are weakly coupled; the magnitude of each cylindrical curvature can be tailored by adjusting prestrain in the EMC on the concave face. An analytical laminated-plate model is developed to calculate the stable shapes of laminates with arbitrary prestrain orientations. For greater computational efficiency, a simplified linear-equivalent constitutive model is developed for prestressed EMCs. Through experimental validation, it is established that quartic polynomials for in-plane strains and out-of-plane deflections are the minimal and sufficient polynomials for the calculation of stable shapes. When the EMCs prestrains are equal, the laminate is bistable over the entire range of prestrain orientations (except at 0°). However, the range of orientations (θ) reduces with a reduction in prestrain ratio. In rectangular bistable laminates, there is a limit on the aspect ratio for a given prestrain (input strain energy) in the EMCs. A study of actuation requirements shows that actuation pressure is minimal in the case of parallel prestressed EMCs and increases with an increase in the angular separation between the EMCs. Actuation pressure is maximum when the EMC on the concave face is at 45° or oriented along the diagonal of the laminate. This study on bistability due to arbitrary prestrain orientations provides the modeling tools and insights that enable the design of morphing structures with complex bistable shapes.

Declaration of Competing Interest

The authors declared no potential conflicts of interest with respect to the research, publication, and authorship of this article.

Data availability statement

The raw/processed data required to reproduce these findings cannot be shared at this time as the data also forms part of an ongoing study.

Acknowledgments

Financial support was provided by the member organizations of the Smart Vehicle Concepts Center, a Phase III National Science Foundation Industry-University Cooperative Research Center (www.SmartVehicleCenter.org) under grant NSF IIP 1738723.

Appendix A. Supplementary data

Supplementary data associated with this article can be found, in the online version, at https://doi.org/10.1016/j.compstruct.2019.111502.

References

[1] Emam SA, Inman DJ. A review on bistable composite laminates for morphing and energy harvesting. Appl Mech Rev 2015;67(6). 060803.
[2] Brinkmeyer A, Santer M, Pirrera A, Weaver PM. Pseudo-bistable self-actuated domes for morphing applications. Int J Solids Struct 2012;49(9):1077–87.
[3] Kebadze E, Guest SD, Pellegrino S. Bistable prestressed shell structures. Int J Solids Struct 2004;41(11–12):2801–20.

[4] Hyer MW. Some observations on the cured shape of thin unsymmetric laminates. J Compos Mater 1981;15(2):175–94.
[5] Daynes S, Potter KD, Weaver PM. Bistable prestressed buckled laminates. Compos Sci Technol 2008;68(15–16):3431–7.
[6] Wang B, Fancey KS. A bistable morphing composite using viscoelastically generated prestress. Mater Lett 2015;158:108–10.
[7] Chillara VSC, Dapino MJ. Mechanically-prestressed bistable composite laminates with weakly coupled equilibrium shapes. Compos Part B: Eng 2017;111:251–60.
[8] Hyer MW. The room-temperature shapes of four-layer unsymmetric cross-ply laminates. J Compos Mater 1982;16(4):318–40.
[9] Hamamoto A, Hyer MW. Non-linear temperature-curvature relationships for unsymmetric graphite-epoxy laminates. Int J Solids Struct 1987;23(7):919–35.
[10] Dano ML, Hyer MW. Thermally-induced deformation behavior of unsymmetric laminates. Int J Solids Struct 1998;35(17):2101–20.
[11] Dano ML, Hyer MW. The response of unsymmetric laminates to simple applied forces. Mech Compos Mater Struct 1996;3(1):65–80.
[12] Hyer MW. Calculations of the room-temperature shapes of unsymmetric laminates. J Compos Mater 1981;15:296–310.
[13] Tawfik S, Tan X, Ozbay S, Armanios E. Anticlastic stability modeling for cross-ply composites. J Compos Mater 2007;41(11):1325–38.
[14] Emam SA. Snapthrough and free vibration of bistable composite laminates using a simplified Rayleigh-Ritz model. Compos Struct 2018;206:403–14.
[15] Jun WJ, Hong CS. Cured shape of unsymmetric laminates with arbitrary lay-up angles. J Reinf Plast Compos 1992;11(12):1352–66.
[16] Bowen CR, Betts DN, Giddings PF, Salo AIT, Kim HAA. Study of bistable laminates of generic lay-up for adaptive structures. Strain 2012;48(3):235–40.
[17] Betts DN, Salo AIT, Bowen CR, Kim HA. Characterisation and modelling of the cured shapes of arbitrary layup bistable composite laminates. Compos Struct 2010;92(7):1694–700.
[18] Murray G, Gandhi F, Bakis C. Flexible matrix composite skins for one-dimensional wing morphing. J Intell Mater Syst Struct 2010;21(17):1771–81.
[19] Bubert EA, Woods BKS, Lee K, Kothera CS, Wereley NM. Design and fabrication of a passive 1D morphing aircraft skin. J Intell Mater Syst Struct 2010;21(17):1699–717.
[20] Chillara VSC, Dapino MJ. Stability considerations and actuation requirements in bistable laminated composites. Compos Struct 2018;184:1062–70.
[21] Reddy JN. Mechanics of laminated composite plates – theory and analysis. Boca Raton, FL: CRC Press; 1997.
[22] Mattioni F, Weaver PM, Potter KD, Friswell MI. The application of thermally induced multistable composites to morphing aircraft structures. The 15th international symposium on: smart structures and materials & nondestructive evaluation and health monitoring. San Diego, CA: International Society for Optics and Photonics; 2008. p. 693012-11.
[23] Udani JP, Arrieta AF. Analytical modeling of multi-sectioned bi-stable composites: stiffness variability and embeddability. Compos Struct 2019;216:228–39.
[24] Tawfik SA, Stefan Dancila D, Armanios E. Planform effects upon the bistable response of cross-ply composite shells. Compos Part A: Appl Sci Manuf 2011;42(7):825–33.
[25] Chillara VSC, Headings LM, Tsuruta R, Itakura E, Gandhi U, Dapino MJ. Shape memory alloy–actuated prestressed composites with application to morphing automotive fender skirts. J Intell Mater Syst Struct 2019;30(3):479–94.
[26] Pirrera A, Avitabile D, Weaver PM. Bistable plates for morphing structures: a refined analytical approach with high-order polynomials. Int J Solids Struct 2010;47(25–26):3412–25.
[27] Potter K, Weaver P, Seman AA, Shah S. Phenomena in the bifurcation of unsymmetric composite plates. Compos Part A: Appl Sci Manuf 2007;38(1):100–6.
[28] Hyer MW. Stress analysis of fiber-reinforced composite materials. DEStech Publications, Inc; 2009.